Combustion and Flame 158 (2011) 240–254

Contents lists available at ScienceDirect

Combustion and Flame

journal homepage: www.elsevier.com/locate/combustflame

Molecular diffusion effects in LES of a piloted methane–air flame

Konstantin A. Kemenov *, Stephen B. Pope

Sibley School of Mechanical and Aerospace Engineering, Cornell University, Ithaca, NY 14853, United States

ARTICLE INFO

Article history:
Received 24 February 2010
Received in revised form 21 April 2010
Accepted 29 August 2010
Available online 24 September 2010

Keywords:
Non-premixed turbulent combustion
Large-eddy simulation
Molecular diffusion
Sandia flame D

ABSTRACT

Molecular diffusion effects in LES of a piloted methane–air (Sandia D) flame are investigated on a series of grids with progressively increased resolution. The reacting density, temperature and chemical composition are modeled based on the mixture fraction approach combined with a steady flamelet model. With a rationale to minimize interpolation uncertainties that are routinely introduced by a flamelet table look-up, quadratic splines relationships are employed to represent thermochemical variables. The role of molecular diffusivity in effecting spatial transport is studied by drawing a comparison with the turbulent diffusivity and analyzing their statistics conditioned on temperature. Statistical results demonstrate that the molecular diffusivity in the near-field almost always exceeds the turbulent diffusivity, except at low temperatures (less than 500 K). Thus, by altering the jet near-field, molecular transport plays an important role in the further downstream jet development. Molecular diffusivity continues to dominate in the centerline region throughout the flow field. Overall, the results suggest the strong necessity to represent molecular transport accurately in LES studies of turbulent reacting flows.

1. Introduction

High-fidelity prediction of non-premixed turbulent flames of practical engineering relevance remains an elusive target in spite of significant advances in the Large-eddy simulation (LES) approach over the past decade. Primarily, this is due to the non-trivial and inherently small-scale character of turbulence–chemistry interactions which is not resolved at the LES grid level and poses well-known modeling challenges. Nevertheless, LES has proved to be a promising simulation approach for a wide range of chemically reacting turbulent flows, including non-premixed turbulent combustion in particular. The number of successful LES applications reported in the literature have been growing and expanding not only in the directions of more and more sophistication in combustion modeling [1–4] but also by adding geometrical complexity of real life gas-turbine combustors [5,6]. A mature methodology which treats the small-scale chemical reaction processes is the transported probability density function (PDF) method [7] which has been successfully applied in the past to a wide range of turbulent non-premixed flames [8,9] in Reynolds-Averaged Navier–Stokes (RANS) simulations. The PDF approach has been extended to LES in the context of the filtered density function (FDF) method [1,10]. Recently, a more mathematically consistent way of extending the PDF method to LES has been proposed by Pope and relies on the concept of the self-conditioned fields (SCF) [11]. Henceforth, we refer to LES/PDF as there is no need in the present context to distinguish between PDF and FDF.

Molecular transport processes play a prominent role in the non-premixed combustion as they control the small-scale molecular mixing and subsequent chemical reactions. Simultaneously, they constitute a major modeling challenge – an accurate and computationally efficient representation of these small-scale processes at the LES grid level. This challenge is not unique for LES. It is even more pronounced in RANS methods. As a result, many existing LES non-premixed combustion modeling approaches are direct copies of their RANS counterparts, albeit with a direct carryover of many RANS modeling assumptions. One such modeling aspect is related to a simplified treatment of molecular diffusion transport.

In the PDF methods molecular diffusion manifests itself through the appearance of the unclosed conditional molecular diffusion term in the PDF evolution equation which makes modeling inevitable. It is important to appreciate that not all molecular diffusion models adopted in the PDF methods provide a "seamless" coupling between LES and PDF solutions at the continuous (non-discrete) formulation level due to the nature of the LES solutions, as was recently discussed by McDermott and Pope [12]. In contrast to the RANS solution, the LES solution, say the resolved mixture fraction field $\tilde{\xi}(\boldsymbol{x},t)$, is a random field and depends on the filter width $\Delta(\boldsymbol{x})$, or more appropriately, on the turbulence resolution length scale, as it explicitly enters models for the subgrid/subfilter (SGS) stress. Thus, it is more appropriate to view the LES solution as a *family* of functions $\{\tilde{\xi}_\Delta\}$ parametrized by Δ rather than a single function. It is very unlikely that a specification of one member of

* Corresponding author.
E-mail address: kak262@cornell.edu (K.A. Kemenov).

0010-2180/$ - see front matter © 2010 The Combustion Institute. Published by Elsevier Inc. All rights reserved.
doi:10.1016/j.combustflame.2010.08.014

a family is sufficient to draw any non-trivial conclusions about the whole LES family [13]. The LES family of solutions has a limiting point – a DNS solution, as the turbulence resolution scale becomes smaller in the DNS limit, i.e., $\Delta/\mathscr{L} \to 0$ for some characteristic flow length scale $\mathscr{L}$. It is important to guarantee that the PDF solution is able to reproduce the same DNS limit. McDermott and Pope [12] provide an example when this is not the case, as well as listing other desirable properties for the PDF diffusion models. Namely, when in the Lagrangian particle representation of the PDF transport equation, the spatial molecular transport is modeled as a stochastic Weiener processes (for the particle position equation), the corresponding scalar variance evolution equation contains a spurious production term that does not vanish in the DNS limit. In other words, there exist some resolution scale Δ – starting from which the LES and PDF SGS variances become inconsistent.

Another frequently adopted RANS assumption is that the molecular properties can be taken to be constants. Although in reactive flows molecular properties are greatly enhanced by the exothermicity of chemical reactions, this assumption can be somewhat justifiable when molecular diffusivity and viscosity are much smaller than their turbulent subgrid scale counterparts. However, in LES this assumption fails as the turbulence resolution scale becomes smaller and smaller. Therefore, it will not lead to the consistent LES/PDF formulation. Clearly, the increased values of molecular diffusivity due to temperature on the one hand, and decreased values of the turbulent SGS diffusivity as the LES grid becomes fine enough on the other, are expected to lead to significant effects of molecular diffusion on the LES statistics of temperature and composition.

Motivated by developing a seamless, numerically accurate LES/PDF strategy to simulate turbulence–chemistry interaction in turbulent flames, our objective in the present paper is to study the role of the molecular diffusivity in LES of a laboratory methane–air flame. To achieve this we compare the molecular and turbulent SGS diffusivities on several grids with progressively increased resolutions, and demonstrate that the molecular diffusivity cannot be neglected and has to be treated accurately enough even for the simplified diffusion formulations involving mixture-averaged diffusivities.

In this work we focus on one of the canonical flame configurations from the TNF flame series – Sandia flame D. This piloted non-premixed methane–air flame has been extensively studied experimentally by Barlow and Frank [14] and by Schneider et al. [15], and, as a result, it represents an ideal benchmark case for testing and developing combustion models in the context of LES. A number of LES studies of Sandia flame D have been performed successfully in the past with combustion models of varying complexity as summarized in Table 1 [16–27]. It is seen from this table that the specification of the molecular diffusivity is rarely reported, or reported with very little details which makes it difficult to quantify its role with respect to the turbulent SGS diffusivity. In addition, with a few exceptions, reported computations were performed on one grid, and as a result, that does not allow one to draw a firm conclusion on the performance of the employed LES combustion and turbulence models. This paper aims to fill this gap in the literature.

Many combustion models employed in LES of flame D center on a mixture fraction based flamelet approach [28]. In such a simplified turbulence/chemistry interaction treatment chemical composition, temperature and density are parametrized by one (or a few) field variables such as the mixture fraction ξ and its scalar dissipation rate, or a specially constructed progress variable [29]. Such a parametrization produces a flamelet table so that all chemical species, temperature and density can be retrieved from the table as needed which relieves the computational burden of solving composition and enthalpy evolution equations. Existence of the mixture fraction can be justified under assumption of equal Lewis numbers for all species. This assumption neglects differences in species molecular diffusivities – a very rare situation for practical combustion regimes. The necessity to treat differential diffusion has been recognized early as a key for improved predictions in turbulent flame simulations [1,30]. For example, in a recent review of the hierarchy of diffusion models [31], Giacomazzi et al. demonstrated that individual species Lewis numbers vary considerably with temperature in non-premixed methane–air flames. Thus, it is highly desirable for LES combustion models to handle differential diffusion effects accurately. In the context of LES/PDF modeling, it is evident that if, for example, the spatial molecular transport is represented by a single stochastic position equation there is no room to account for different species diffusion coefficients [12].

In spite of shortcomings in representing realistic combustion chemistry, the flamelet parametrization can be a useful tool in the study of particular effects of subgrid scale and/or combustion models on the LES solution. In an attempt to account for differential diffusion effects while retaining the simplicity of the flamelet model, Pitsch and Peters [32] introduced the mixture fraction as a solution of a transport equation with independently specified mixture fraction diffusion coefficient based on the assumption of equal thermal and mixture fraction diffusivities. Here, we follow a similar simplified approach by representing the chemistry by a

Table 1
Specification of the molecular viscosity and mixture fraction (or species) diffusivity in recent LES studies of Sandia flame D. LFM, Lagrangian flamelet model; UFM, unsteady flamelet equation model; LSF, laminar steady flamelet model; FGM, flamelet generated manifold; FT, flamelet table; pPDF, presumed probability density function (beta-pdf or products involving beta-pdf); FDF, filtered density function; EPDF, Eulerian probability density function; CSE, conditional source term estimation model; TF, thickened flame model; rCH, reduced chemical mechanism; SL, Sutherland's law; n.r., not reported.

Authors	Chem./turb. model	Viscosity, $\bar{\mu}$	Diffusivity, $\widetilde{\mathscr{D}}$ or $\bar{\rho}\widetilde{\mathscr{D}}$	*Sc* number $\bar{\mu}/\bar{\rho}\widetilde{\mathscr{D}}$	Grid cells, 10^6
Pitsch and Steiner [16]	LFM/pPDF	n.r.	$\widetilde{\mathscr{D}} \sim \widetilde{T}^{1.7}$	n.r.	1.01
Pitsch [17]	UFM/pPDF	n.r.	$\widetilde{\mathscr{D}} \sim \widetilde{T}^{1.7}$	n.r.	1.01
Kempf et al. [18]	LSF/pPDF	FT	n.r.	n.r.	1.97, 1.97
Sheikhi et al. [19]	LSF/FDF	$\sim \widetilde{T}^{0.7}$	–	0.75	0.93
Mustata et al. [20]	rCH/EPDF	n.r.	n.r.	n.r.	0.49, 1.00
Raman and Pitsch [21]	rCH/FDF	n.r.	n.r.	n.r.	1.05
James et al. [22]	rCH/FDF	n.r.	n.r.	1.0	1.14
Chen [23]	LSF/EPDF	n.r.	n.r.	n.r.	0.28
Ihme and Pitsch [24]	LSF/pPDF	FT	FT	–	2.6
Clayton and Jones [25]	LSF/pPDF	Const.	n.r.	n.r.	1.03
Ferraris and Wen [26]	LSF/CST	n.r.	n.r.	n.r.	1.6
Vreman et al. [27]	FGM/pPDF,TF	SL	$\bar{\rho}\widetilde{\mathscr{D}} \sim \widetilde{T}^{0.69}$	–	1.23, 5.24

single mildly-strained steady flamelet based on physical space integration of steady axisymmetric governing equations describing counter-flow diffusion flame. A flamelet solution is obtained from the OPPDIF module of CHEMKIN with the multi-component formulation for diffusion velocities and the detailed GRI-Mech 3.0 chemical mechanism. Then, mixture transport properties, such as molecular viscosity and diffusivity of the mixture fraction, are computed from the flamelet solution and are fitted to a power law form in temperature, before being used in the LES equations. This allows the model to account for the variation of Schmidt number with temperature. Instead of forming a flamelet table, we approximate the flamelet solution for specific volume and temperature by a quadratic B-spline with respect to the mixture fraction. These approximations allow to eliminate possible flamelet table interpolation errors. This is especially important for low-Mach number projection methods where strong coupling among density, velocity and pressure could cause small table interpolation errors in density to propagate and produce large errors in velocity and scalar fields [33]. Thus, the main objective of the current work is to use a simple, tabulation free combustion model to study resolution effects on statistics of molecular diffusivity as well as the interplay between molecular and subgrid diffusivities in different regions of flame D.

The paper is organized as follows: in Section 2, we present the LES governing equation. An extra scalar equation for the variance of the mixture fraction is needed to compute the resolved values of density and temperature from the quadratic spline model. In Section 3, we introduce the combustion model based on the quadratic spline approximation. We show that a small number of splines are required (typically about 3) for the accurate approximation of density, temperature and major species. Here, we propose a model for the SGS temperature variance which is used as an estimator for the residual contribution to the total temperature variance. While the resolved temperature depends on the first two moments of the mixture fraction according to the quadratic spline approximation, its variance contains terms involving the differences that depend on the third $(\widetilde{\xi^3}-\tilde{\xi}\widetilde{\xi^2})$ and the fourth $(\widetilde{\xi^4}-\widetilde{\xi^2}\,\widetilde{\xi^2})$ moments. We model these differences employing the beta-pdf which conveniently allows all higher moments to be related to the first two. Computational implementation is discussed in Section 4. We present results in Section 5 primarily focusing on temperature and diffusivity. Since the molecular diffusivity is a function of temperature we discuss the temperature field first and compare it with available experimental data [14,15]. Conclusions are drawn in Section 6.

2. Governing equations

In LES of variable-density turbulent flows with parametrized chemistry one solves evolution equations for large-scale resolved quantities, namely the density $\bar{\rho}$, the density weighted velocity $\tilde{u}_i$, pressure $\bar{p}$ and the mixture fraction $\tilde{\xi}$ (here, the common Favre notation for the density weighted resolved quantity is used, i.e., $\tilde{\xi}=\overline{\rho\xi}/\bar{\rho}$). The flamelet-based simplified treatment of turbulence–chemistry interaction requires additional equations that describe the thermochemical state of the system and functionally relate the resolved density, temperature and species mass fraction with the mixture fraction field $\tilde{\xi}$ and its subgrid scale (SGS) variance $V_\xi=\widetilde{\xi^2}-(\tilde{\xi})^2$. The dependence of the resolved thermochemical fields on the SGS mixture fraction variance accounts for the effect of residual fluctuations and makes it an important modeling variable in LES of non-premixed combustion systems. While there are different ways to model the SGS mixture fraction variance [34], in this work we integrate an extra transport equation for V_ξ. Accordingly, the LES system of the governing equations is given by:

$$\frac{\partial\bar{\rho}}{\partial t}+\frac{\partial\bar{\rho}\tilde{u}_j}{\partial x_j}=0, \tag{1}$$

$$\frac{\partial\bar{\rho}\tilde{u}_i}{\partial t}+\frac{\partial\bar{\rho}\tilde{u}_i\tilde{u}_j}{\partial x_j}=-\frac{\partial\bar{p}}{\partial x_i}+2\frac{\partial}{\partial x_j}\left((\bar{\mu}+\mu_T)\left(\widetilde{S}_{ij}-\frac{1}{3}\widetilde{S}_{kk}\delta_{ij}\right)\right), \tag{2}$$

$$\frac{\partial\bar{\rho}\tilde{\xi}}{\partial t}+\frac{\partial\bar{\rho}\tilde{u}_j\tilde{\xi}}{\partial x_j}=\frac{\partial}{\partial x_j}\left(\bar{\rho}(\widetilde{\mathscr{D}}+\mathscr{D}_T)\frac{\partial\tilde{\xi}}{\partial x_j}\right), \tag{3}$$

$$\frac{\partial\bar{\rho}V_\xi}{\partial t}+\frac{\partial\bar{\rho}\tilde{u}_jV_\xi}{\partial x_j}=\frac{\partial}{\partial x_j}\left(\bar{\rho}(\widetilde{\mathscr{D}}+\mathscr{D}_T)\frac{\partial V_\xi}{\partial x_j}\right)-2\bar{\rho}\tilde{\chi}_\xi+2\bar{\rho}(\widetilde{\mathscr{D}}+\mathscr{D}_T)\frac{\partial\tilde{\xi}}{\partial x_j}\frac{\partial\tilde{\xi}}{\partial x_j}, \tag{4}$$

$$\bar{\rho}=\bar{\rho}(\tilde{\xi},V_\xi),\ \widetilde{T}=\widetilde{T}(\tilde{\xi},V_\xi),\ \bar{\mu}=\overline{\mu(T)},\ \bar{\rho}\widetilde{\mathscr{D}}=\overline{\rho\mathscr{D}(T)}, \tag{5}$$

with $\widetilde{S}_{ij}$ and $\tilde{\chi}_\xi$ being the resolved strain rate and scalar dissipation rate, respectively. The filtered diffusive flux in the scalar transport equations is simplified as $\overline{\rho\mathscr{D}\nabla\xi}=\bar{\rho}\widetilde{\mathscr{D}\nabla\xi}\approx\bar{\rho}\widetilde{\mathscr{D}}\nabla\tilde{\xi}$ – a questionable but standard practice in combustion LES [35]. On the other hand, subgrid scale contributions arising from nonlinearities in molecular properties can be accounted for once the SGS temperature variance is available. This is further discussed in Section 3.3.

In the LES momentum equation, Eq. (2), the Smagorinsky model is used to obtain the deviatoric part of the unclosed SGS stress $\tau_{ij}=\bar{\rho}\tilde{u}_i\tilde{u}_j-\bar{\rho}\widetilde{u_iu_j}$:

$$\tau_{ij}-\frac{\delta_{ij}}{3}\tau_{kk}=2\mu_T\left(\widetilde{S}_{ij}-\frac{\delta_{ij}}{3}\widetilde{S}_{kk}\right), \tag{6}$$

with the eddy viscosity being $\mu_T=\bar{\rho}C_S\Delta^2|\widetilde{S}|$ and $|\widetilde{S}|=(2\widetilde{S}_{ij}\widetilde{S}_{ij})^{1/2}$. Here, a model constant C_S is computed according to the Germano dynamic procedure [36] with Lilly's modification [37]. In addition, a commonly used averaging operation in the periodic direction is employed for the numerator and denominator in the expression for C_S. In both scalar equations, Eqs. (3) and (4), the unclosed subgrid scalar flux is modeled by a standard gradient diffusion hypothesis with the same subgrid diffusivity $\bar{\rho}\mathscr{D}_T$ for both scalar fields, for example for the mixture fraction one has:

$$\bar{\rho}\tilde{u}_i\tilde{\xi}-\bar{\rho}\widetilde{u_i\xi}=\bar{\rho}\mathscr{D}_T\frac{\partial\tilde{\xi}}{\partial x_i}. \tag{7}$$

The subgrid diffusivity is specified based on the eddy viscosity and the subgrid Schmidt number as $\bar{\rho}\mathscr{D}_T=\mu_T/Sc_T$ with a commonly used value of $Sc_T=0.4$ [16].

Finally, the scalar dissipation rate term $2\bar{\rho}\tilde{\chi}_\xi$ in Eq. (4) is decomposed into resolved and SGS parts where the latter is taken to be proportional to the SGS mixture fraction variance:

$$2\bar{\rho}\tilde{\chi}_\xi=2\bar{\rho}\widetilde{\mathscr{D}}\frac{\partial\tilde{\xi}}{\partial x_j}\frac{\partial\tilde{\xi}}{\partial x_j}+C\frac{\bar{\rho}\mathscr{D}_TV_\xi}{\Delta^2}, \tag{8}$$

with a model constant chosen to be $C=2$. This is consistent with the linear relaxation model for the SGS dissipation rate used in other LES studies of methane jet flames, such as the Cabra lifted flame by Domingo et al. [38] ($C=1.8$), and piloted Sandia flames by Ihme and Pitsch [24] ($C=11.25$). We found that while having a negligible effect on the resolved mixture fraction variance the higher values of C lead to reduced values of the SGS variance in the jet near-field thus diminishing effects of the small-scale scalar mixing. In a more general way, the model constant C can be also evaluated from a dynamic procedure as discussed, for example, by Pera et al. [34]. Substitution of Eq. (8) results in cancellation of the production term in Eq. (4) that simplifies to the final form:

$$\frac{\partial\bar{\rho}V_\xi}{\partial t}+\frac{\partial\bar{\rho}\tilde{u}_jV_\xi}{\partial x_j}=\frac{\partial}{\partial x_j}\left(\bar{\rho}(\widetilde{\mathscr{D}}+\mathscr{D}_T)\frac{\partial V_\xi}{\partial x_j}\right)+2\bar{\rho}\mathscr{D}_T\frac{\partial\tilde{\xi}}{\partial x_j}\frac{\partial\tilde{\xi}}{\partial x_j}-\frac{C\bar{\rho}\mathscr{D}_T}{\Delta^2}V_\xi. \tag{9}$$

3. Combustion model

3.1. Specification of molecular properties

Molecular transport properties in Eq. (5) are obtained from a steady laminar flamelet solution with the detailed GRI-Mech 3.0

chemical mechanism by the OPPDIF module of CHEMKIN 4.1 and its transport database. A mildly-strained flamelet with a nominal strain rate of $a = 50\ s^{-1}$ is computed in a 1D axisymmetric counter-flow configuration with the full multi-component formulation for transport coefficients. The mixture averaged molecular viscosity is then computed by Wilke's semi-empirical formula [39]:

$$\mu = \sum_{k=1}^{N} \frac{X_k \mu_k}{\sum_{j=k}^{N} X_j \Phi_{kj}}, \quad \text{where}$$

$$\Phi_{kj} = \frac{1}{\sqrt{8}} \left(1 + \frac{W_k}{W_j}\right)^{-\frac{1}{2}} \left[1 + \left(\frac{\mu_k}{\mu_j}\right)^{\frac{1}{2}} \left(\frac{W_j}{W_k}\right)^{1/4}\right]^2, \tag{10}$$

here, X_k, W_k and μ_k are mole fraction, molecular weight and viscosity of the kth species, respectively. The mixture fraction molecular diffusivity is computed from the mixture-averaged specific heat capacity and thermal conductivity ($\rho D = \lambda / C_p$), thus employing the unity Lewis number assumption for the mixture fraction. The mixture averaged thermal conductivity is given by:

$$\lambda = \frac{1}{2}\left(\sum_{k=1}^{N} X_k \lambda_k + \frac{1}{\sum_{k=1}^{N} X_k / \lambda_k}\right). \tag{11}$$

The mixture averaged molecular transport properties are then fitted to a power-law form with respect to temperature as follows:

$$\mu(T) = 1.75 \times 10^{-5} \left(\frac{T}{T_0}\right)^{0.69}, \tag{12}$$

$$\rho D(T) = 2.48 \times 10^{-5} \left(\frac{T}{T_0}\right)^{0.72} \left(\frac{\text{kg}}{\text{m} \cdot \text{s}}\right), \tag{13}$$

with $T_0 = 298$ K. Similar excellent approximations of the CHEMKIN data can be obtained using quadratic functions of the following form:

$$\mu(T) = a_\mu + b_\mu \left(\frac{T}{T_0}\right) + c_\mu \left(\frac{T}{T_0}\right)^2, \tag{14}$$

$$\rho D(T) = a_D + b_D \left(\frac{T}{T_0}\right) + c_D \left(\frac{T}{T_0}\right)^2, \tag{15}$$

where $c_\mu = -3.2 \times 10^{-7}$, $b_\mu = 1.08 \times 10^{-5}$, $a_\mu = 7.3 \times 10^{-6}$ (kg/m s) and $c_D = -4.3 \times 10^{-7}$, $b_D = 1.6 \times 10^{-5}$, $a_D = 9.5 \times 10^{-6}$ (kg/m s), respectively. The latter approximation allows us to account for the effects of temperature fluctuations on molecular properties as further outlined in Section 3.3. The functional dependence of the mixture molecular properties on temperature for both models is compared with the corresponding CHEMKIN data in Fig. 1a and b. Note that the molecular properties extracted from the CHEMKIN flame calculation are double-valued functions of temperature – with one value on the lean side and one on the rich side of the peak temperature. However, these properties are adequately approximated by the single-valued power laws, Eqs. (12)–(15).

3.2. Approximation of resolved density and temperature

It is standard practice in flamelet-based approaches to use a presumed pdf, such as the beta-pdf, to obtain LES Favre-filtered resolved quantities [40]. Consequently, in the simplest case, the resolved LES fields are viewed as expectations (means) with respect the beta-pdf which is parametrized by the resolved mixture fraction and its SGS variance. Additional hypotheses are needed if the thermochemical state is parametrized by extra variables such as the scalar dissipation rate or the progress variable to represent a joint form of a presumed pdf [29]. For practical purposes, all thermochemical variables are tabulated and stored in a multidimensional table spanned by at least two variables, i.e., $\tilde{\xi}$ and V_ξ, in order to retrieve them at run time.

In this work we adopt a different approach which is based on simple algebraic relations between the resolved mixture fraction, the SGS variance on the one hand and the resolved thermochemical variables on the other. In particular, in order to avoid possible interpolation errors associated with a flamelet table, as well as for simplicity, we use smooth functional approximation of thermochemical variables based on quadratic B-splines. This approach allows to obtain the resolved LES quantities based on definition of the Favre filtering and naturally includes the SGS mixture fraction variance in the formulation.

We first note that for the specific volume v we have $\tilde{v} = \widetilde{1/\rho} = 1/\bar{\rho}$ resulting in a useful expression for the filtered density $\bar{\rho} = \tilde{v}^{-1}$. In the context of flamelet-based modeling we represent the flamelet parametrization $v(\xi)$ at the resolved scale as $\tilde{v}(\tilde{\xi}, V_\xi)$. Note that if the subgrid fluctuations are absent then $\tilde{v}(\tilde{\xi}, 0) = v(\tilde{\xi})$. In the present approach our purpose is to obtain a simple expression for $\tilde{v}(\tilde{\xi}, V_\xi)$ (and other thermochemical variables) based on a given functional form of the flamelet $v(\xi)$. In its simplest form a quadratic B-spline approximation to the flamelet function $v(\xi)$ is represented by a single quadratic function $v_o(\xi) = a + b\xi + c\xi^2$. This translates in the following approximation for the resolved specific volume $\tilde{v}$:

$$\tilde{v}_o(\tilde{\xi}, V_\xi) = a + b\tilde{\xi} + c\widetilde{\xi^2} = a + b\tilde{\xi} + c(\tilde{\xi}^2 + V_\xi) = \tilde{v}(\tilde{\xi}, 0) + cV_\xi, \tag{16}$$

where the coefficients a, b and c can be found by fitting to the CHEMKIN flamelet data for specific volume. This is shown in Fig. 2a and b. Here, the mixture fraction is defined according to Bilger et al. [41]. It is seen that a single parabola representation provides an adequate approximation for lean mixtures while slightly underpredicting the density for rich mixtures. For temperature, however, the quadratic approximation is less convincing, as it is evident from Fig. 3a where it is shown by a dashed line. The spline approximation of a flamelet function can be improved if one considers a piece-wise quadratic approximation based on a quadratic B-spline $\tilde{v}(\tilde{\xi}, 0) = v_s(\tilde{\xi})$. For example, a spline approximation of the specific volume which consists of three smoothly connected parabolic pieces is shown in Fig. 2a and can be written as:

$$v_s(\xi) = \sum_{i=1}^{n} c_i B_{i,2}(\xi), \tag{17}$$

where $\{B_{i,2}\}_{i=1}^{n}$ are quadratic B-splines, c_i are control points and $n = 5$. The jth B-spline of degree $d = 2$ (quadratic) is fully defined by its knots sequence $(\xi_j)_{j=1}^{n+d+1}$ according to the following recurrence relationship:

$$B_{j,d}(\xi) = \frac{\xi - \xi_j}{\xi_{j+d} - \xi_j} B_{j,d-1}(\xi) + \frac{\xi_{j+1+d} - \xi}{\xi_{j+d+1} - \xi_{j+1}} B_{j+1,d-1},$$
$$B_{j,0}(\xi) = \begin{cases} 1, & \text{if } \xi_j \leqslant \xi < \xi_{j+1} \\ 0, & \text{otherwise.} \end{cases} \tag{18}$$

The knot sequence $(\xi_j)_{j=1}^{8}$ and control points $(c_i)_{i=1}^{5}$ used to define the quadratic B-spline approximations of the specific volume and temperature are given in Table 2. The approximation for the resolved specific volume is then can be defined as:

$$\tilde{v}(\tilde{\xi}, V_\xi) = \tilde{v}(\tilde{\xi}, 0) \frac{\tilde{v}_o(\tilde{\xi}, V_\xi)}{\tilde{v}_o(\tilde{\xi}, 0)}. \tag{19}$$

The basic assumption here is that the ratio of the resolved specific volumes computed at non-zero and zero variances according to the spline approximation is equal to the same ratio which is computed based on the simple quadratic approximation, i.e., $\tilde{v}(\tilde{\xi}, V_\xi)/\tilde{v}(\tilde{\xi}, 0) = \tilde{v}_o(\tilde{\xi}, V_\xi)/\tilde{v}_o(\tilde{\xi}, 0)$. In Eq. (19), a prefactor $\tilde{v}(\tilde{\xi}, 0) = v_s(\tilde{\xi})$ defines a shape of the resolved flamelet profile, while the ratio $\tilde{v}_o(\tilde{\xi}, V_\xi)/\tilde{v}_o(\tilde{\xi}, 0)$ controls the magnitude that depends on the SGS mixture fraction variance.

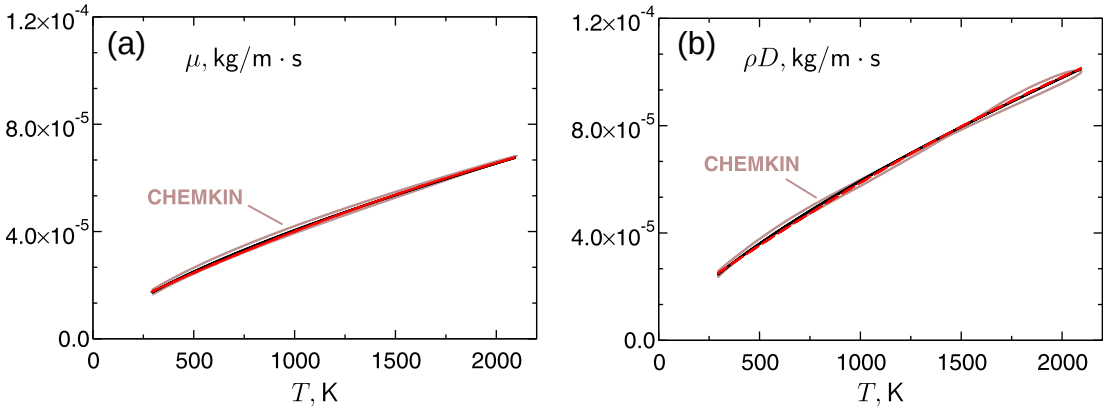

Fig. 1. Molecular viscosity (a) and diffusivity (b) as functions of temperature in the laminar flame calculations: light line – CHEMKIN; solid line – power-law approximations, Eqs. (12) and (13); dashed line – quadratic approximations, Eqs. (14) and (15).

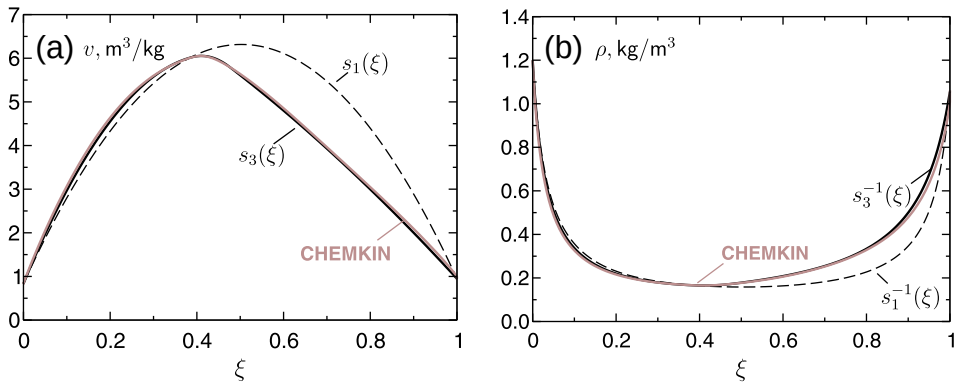

Fig. 2. (a) Specific volume vs. mixture fraction. Quadratic spline approximations of the CHEMKIN flamelet solution – $s_1(\xi)$, $s_3(\xi)$ employing 1 and 3 parabolic pieces, respectively; (b) density vs. mixture fraction.

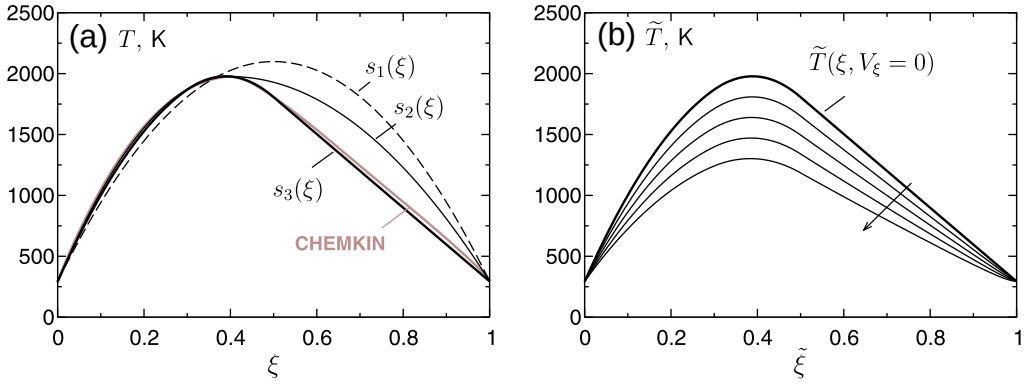

Fig. 3. Temperature vs. mixture fraction: (a) quadratic spline approximations of the CHEMKIN flamelet solution – $s_1(\xi)$, $s_2(\xi)$, $s_3(\xi)$ employing 1,2 and 3 parabolic pieces, respectively; (b) dependence of the resolved temperature $\widetilde{T}$ on turbulent fluctuations of the mixture fraction represented by the SGS variance $V_\xi = \alpha\tilde{\xi}(1-\tilde{\xi})$ with $\alpha = 0$, 0.1, 0.2, 0.3, 0.4 (in descending order).

Table 2
The knot sequence $(\xi_j)_{j=1}^{8}$ and control points $(c_i)_{i=1}^{5}$ for B-spline approximations of specific volume and temperature. Last three columns of two bottom rows show coefficients *a*, *b*, *c* for the corresponding quadratic approximations.

	ξ_1	ξ_2	ξ_3	ξ_4	ξ_5	ξ_6	ξ_7	ξ_8
$v_s(\xi)$	0	0	0	0.390	0.474	1	1	1
$T_s(\xi)$	0	0	0	0.297	0.498	1	1	1
	c_1	c_2	c_3	c_4	c_5	a	b	c
$v_s(\xi)$ (m^3/kg)	0.834	5.543	6.131	3.801	0.947	0.833	21.94	−21.82
$T_s(\xi)$ (K)	291	1481	2117	1051	294	291	7226	−7223

Similar expressions can be applied to other thermochemical variables. The effect of the non-zero variance on the resolved temperature profile computed analogously to Eq. (19) is shown in Fig. 3b for several different values of V_ξ. It may be seen that the resolved flamelet temperature continuously decreases while retaining the asymmetry with respect to lean and rich parts of the mixture. Finally, we would like to point out that in the simple combustion model used, we deliberately do not introduce an assumed PDF. However, the resolved property defined by Eq. (19) may be associated with an implied PDF, although such a PDF is almost certainly not unique.

3.3. Modeling of SGS temperature variance

Ultimately, an LES aims to produce the LES statistics Q^m, such as the statistical mean or variance, which would give an accurate estimation of the true statistics Q of some turbulent quantity of interest. For example, Q^m can be the estimation of the mean temperature $Q = \langle T\rangle$ or temperature variance $Q = \langle T^2\rangle - \langle T\rangle^2$. As pointed out by Pope [13], the LES statistics estimation Q^m can be decomposed as $Q^m = Q^W + Q^r$, where Q^W is defined solely by the resolved LES fields, while Q^r estimates the contribution from the unresolved (residual) motions. Thus, it is desirable for an LES model to provide a procedure for estimation of the residual component Q^r. While the mean of the resolved LES fields can provide a reasonable estimation for the total statistical mean in free-shear flows, the variance estimation requires more careful accounting of the residual scale contribution. The mean SGS variance provides a natural model for an estimation of the residual contribution Q^r:

$$Q = \langle T^2\rangle - \langle T\rangle^2 \approx Q^m = \langle(\widetilde{T})^2\rangle - \langle\widetilde{T}\rangle^2 + \langle V_T\rangle, \quad \text{with}$$
$$V_T = \widetilde{T^2} - (\widetilde{T})^2. \tag{20}$$

The analytical form of the resolved flamelet temperature allows one to obtain a model for the SGS temperature variance from its definition. Let $T_o(\xi) = a_T + b_T\xi + c_T\xi^2$ and $T_s(\xi)$ be the quadratic and spline approximations, respectively. Then similar to Eq. (19) one could approximate the resolved temperature as:

$$\widetilde{T}(\tilde{\xi}, V_\xi) = \widetilde{T}(\tilde{\xi}, 0)\frac{\widetilde{T}_o(\tilde{\xi}, V_\xi)}{\widetilde{T}_o(\tilde{\xi}, 0)}, \tag{21}$$

where $\widetilde{T}(\tilde{\xi}, 0) = T_s(\tilde{\xi})$. Since the ratio $\widetilde{T}(\tilde{\xi}, 0)/\widetilde{T}_o(\tilde{\xi}, 0)$ does not account for any turbulent fluctuations being independent of the variance, from the definitions of V_T and T_o it follows that:

$$V_T = \frac{\widetilde{T}^2(\tilde{\xi}, 0)}{\widetilde{T}_o^2(\tilde{\xi}, 0)}\left[\widetilde{T_o^2} - (a_T + b_T\tilde{\xi} + c_T\widetilde{\xi^2})^2\right]$$
$$= \frac{\widetilde{T}^2(\tilde{\xi}, 0)}{\widetilde{T}_o^2(\tilde{\xi}, 0)}\left[b_T^2 V_\xi + 2b_T c_T(\widetilde{\xi^3} - \tilde{\xi}\widetilde{\xi^2}) + c_T^2(\widetilde{\xi^4} - \widetilde{\xi^2}\,\widetilde{\xi^2})\right]. \tag{22}$$

Further simplification is necessary since the third ($\widetilde{\xi^3}$) and the fourth ($\widetilde{\xi^4}$) SGS raw moments of the mixture fraction are unknown and need to be modeled in terms of V_ξ and $\tilde{\xi}$. The simplest way to estimate the higher moments of the mixture fraction field is to use the beta-pdf assumption. Thus, our approximation model for the SGS temperature variance V_T is based on the beta-pdf which is widely used in presumed pdf modeling of the mixture fraction field in non-premixed turbulent combustion [29,40].

Accordingly, the LES fields are viewed as statistical means with respect to the beta-pdf distribution. The two-parameter beta-pdf $P_\beta(\xi; a, b)$ is fully defined by its mean $\tilde{\xi}$ and variance V_ξ through $a = \tilde{\xi}[\tilde{\xi}(1-\tilde{\xi})/V_\xi - 1]$ and $b = a/\tilde{\xi} - a$. An attractive feature of the beta-pdf distribution is that it allows the higher moments to be related to the mean and variance by a simple recurrence formula:

$$\widetilde{\xi^3} = \left[\frac{(\tilde{\xi}^2 + V_\xi)(1-\tilde{\xi}) + V_\xi}{\tilde{\xi}(1-\tilde{\xi}) + V_\xi}\right]\widetilde{\xi^2},$$
$$\widetilde{\xi^4} = \left[\frac{(\tilde{\xi}^2 + V_\xi)(1-\tilde{\xi}) + 2V_\xi}{\tilde{\xi}(1-\tilde{\xi}) + 2V_\xi}\right]\widetilde{\xi^3}. \tag{23}$$

Note that if the mixture fraction variance is equal to zero then $\widetilde{\xi^3} = \tilde{\xi}\widetilde{\xi^2}$ and $\widetilde{\xi^4} = \widetilde{\xi^2}\,\widetilde{\xi^2}$ resulting in zero SGS temperature variance according to Eq. (22).

The SGS temperature variance allows us to account for the effect of the subgrid temperature fluctuations on molecular properties, thus avoiding usual modeling approximations $\widetilde{D(T)} = D(\widetilde{T})$ and $\widetilde{\mu(T)} = \mu(\widetilde{T})$. For example, from Eq. (15) the resolved diffusivity can be written as

$$\bar{\rho}\widetilde{D(T)} = a_D + \frac{b_D}{T_0}\widetilde{T} + \frac{c_D}{T_0^2}\widetilde{T^2} = a_D + \frac{b_D}{T_0}\widetilde{T} + \frac{c_D}{T_0^2}(\widetilde{T}^2 + V_T). \tag{24}$$

However, as can be seen from Fig. 1b $\rho D(T)$ is almost linear in T, and hence, a significant difference between $\bar{\rho}\widetilde{D(T)}$ and $\bar{\rho}D(\widetilde{T})$ is not expected.

4. Computational configuration

We apply LES Eqs. (1)–(5) to simulate Sandia flame D that is shown schematically in Fig. 4, and which has been studied experimentally by Barlow and Frank [14]. The fuel jet consists of a mixture of 25% methane and 75% air (by volume) and emanates from a nozzle with diameter $D = 7.2$ mm at a bulk velocity of $U_b = 49.6$ m/s, which defines a characteristic Reynolds number of $Re = 22{,}400$. The nozzle is surrounded by a coaxial pilot nozzle with a diameter of 2.62D. The pilot flow is a lean burnt mixture of C_2H_2, air, CO_2, H_2 and N_2 corresponding to a mixture fraction value of $\xi = 0.271$, with a bulk velocity of 11.4 m/s. The coaxial burner is further surrounded by co-flowing air with a bulk velocity of 0.9 m/s.

In this work the modeled flow configuration is studied in a cylindrical computational domain of $120.3D \times 20D \times 2\pi$ that is represented in cylindrical coordinates (x, r, θ) as depicted in Fig. 4. In the simulations the jet and pilot nozzles have a small axial extension of $0.3D$ upstream of the nozzle exit plane, which is taken as the origin of the axial coordinate, x. The dimensions of the computational domain as well as flow variables are non-dimensionalized by the characteristic jet parameters (i.e., diameter, bulk velocity, density). The turbulent jet inflow velocity condition is generated separately by running a high resolution LES of the stationary turbulent pipe flow enforcing the experimental mean and rms of axial velocity as measured by the TU Darmstadt group [15]. The turbulent pipe flow simulation has been conducted on a $192 \times 96 \times 96$ grid with periodic boundary conditions in the streamwise direction. Accumulated velocity field data are saved and used to generate inflow conditions by linear interpolation onto the LES grid at the jet inlet plane. The inflow velocity condition for the pilot is based on the measured mean with the superimposed uncorrelated random noise fluctuations of low intensity (~1%) according to the measured rms profiles, while in the co-flow region the measured bulk values with zero turbulent intensity are used. The mixture fraction field is prescribed as a step function according to an experimental value of $\tilde{\xi} = 0.271$ for the pilot, and $\tilde{\xi} = 1$ and $\tilde{\xi} = 0$ for the jet and co-flow, respectively. Finally, the convective boundary conditions are employed for velocity and scalar fields on the outflow boundary including the entrainment boundary of the computational domain.

A structured Stanford LES code is employed to solve the variable-density LES equations, Eqs. (1)–(5), written in cylindrical coordinates [29]. The numerical method is second-order accurate in space and time and adopts an energy-conserving discretization

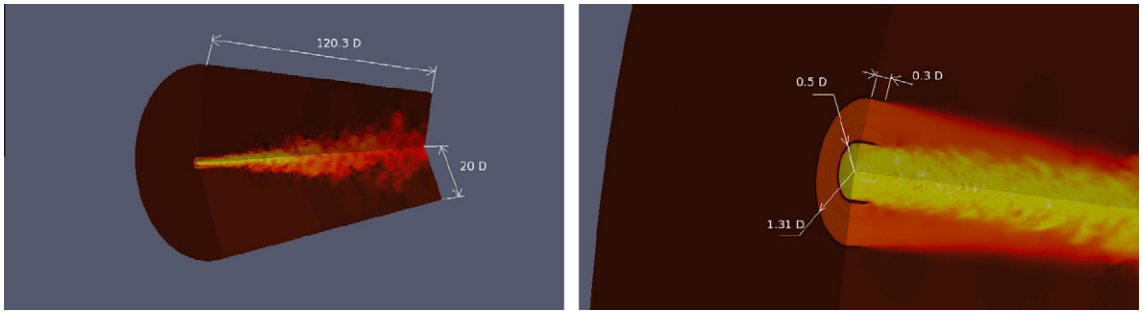

Fig. 4. Computational domain and geometrical configuration of Sandia flame D.

scheme for the momentum equation. Scalar transport equations are discretized using the QUICK scheme [42] and solved employing a semi-implicit iterative technique, which has proven to be effective for typical low-Mach combustion problems [29]. Domain decomposition is used for the LES code parallelization.

In this work we employ five grids $G1,\ldots,G5$ with a progressively increasing resolution from about 0.2 to 10.5 million cells as detailed in Table 3. All grids are stretched in the axial direction as well as in the radial direction, with clustering in the jet nozzle and pilot annulus regions, while remaining uniformly spaced in the circumferential direction. Grid resolution parameters for the jet nozzle and the pilot are given in Table 4. In all simulations, with the exception of the finest grid $G5$, a zero state is employed as the initial condition for all scalar variables except the velocity field, which is taken to be uniform and equal to the co-flow velocity in the whole domain. For the finest grid, the initial fields are interpolated from a statistically stationary solution on the preceding grid $G4$. Time integration is performed with a variable time step corresponding to a CFL number of 0.3–0.35. Statistics are accumulated after the simulation has reached a statistically stationary state which is verified by convergence in the rms statistics. This corresponds to about 10 flow-through times based on the jet averaged centerline velocity and the characteristic length of $L = 75D$, $(t_{fl} = \int_0^L dx/\langle\widetilde{U}\rangle(x))$. Such a defined flow-through time is about two times larger than a time computed based on the bulk velocity value ($t_B = L/U_B$). After that, the simulation is continued for approximately four flow-through times to accumulate statistics. The LES statistics are computed by averaging in time and the circumferential direction, and these averages are denoted by angular brackets, e.g., $\langle\widetilde{T}\rangle$.

Table 3
Grid parameters and the minimum/maximum cell width in the axial and radial directions.

Grid	Resolution (x,r,θ)	Cells, 10^6	$\Delta^x_{\min}$	$\Delta^x_{\max}$	$\Delta^r_{\min}$	$\Delta^r_{\max}$
$G1$	$96\times64\times32$	0.196	12×10^{-2}	4.78	2.8×10^{-2}	1.96
$G2$	$160\times96\times64$	0.983	7.3×10^{-2}	2.89	1.8×10^{-2}	1.33
$G3$	$256\times128\times64$	2.097	4.5×10^{-2}	1.81	1.4×10^{-2}	1.01
$G4$	$256\times192\times96$	4.719	4.5×10^{-2}	1.81	9.4×10^{-3}	0.67
$G5$	$320\times256\times128$	10.485	3.6×10^{-2}	1.45	7.0×10^{-3}	0.51

Table 4
Grid resolutions for the jet nozzle and the pilot.

Grid	Cells in x for $x<0$	Cells in r for jet nozzle	Cells in r for pilot	Cells in jet nozzle wall	Cells in pilot wall
$G1$	3	10	15	2	2
$G2$	5	15	22	3	3
$G3$	8	20	30	3	4
$G4$	8	30	45	4	6
$G5$	9	40	50	5	7

5. Results and discussion

5.1. Resolution and modeling considerations

Before proceeding with the analysis of molecular diffusivity and other scalar fields we first discuss simple resolution indicators on different grids. A standard way to assess the achieved resolution in a particular simulation is to compare the statistics of the resolved motion, i.e., the turbulent kinetic energy (TKE) $k_{res} = 1/2(\langle\tilde{u}_j^2\rangle - \langle\tilde{u}_j\rangle^2)$ with that of the residual motion $\langle k_{sgs}\rangle$. Then, different resolution measures can be formed based on the ratio of $\langle k_{sgs}\rangle$ and k_{res} or their algebraic combinations [13,43]. The quality of such measures relies on the quality of the SGS turbulent kinetic energy estimation. In the present work, we do not integrate an evolution equation for k_{sgs} explicitly, so a simple scaling based relation $k_{sgs} \sim (|\widetilde{S}|\Delta)^2 \sim (\nu_T/\Delta)^2$ is used which results in the following expression, $k_{sgs} = (\nu_T/C_M\Delta)^2$. Here, Δ is the characteristic cell size and C_M is chosen to be 0.069 similar to an LES study of Boudier et al. [6].

Figure 5 shows radial profiles of k_{res} and $\langle k_{sgs}\rangle$ for axial locations of $x = 7.5D, 15D, 45D$, and for the characteristic size based on the cell volume $\Delta = (\Delta_x r\Delta_\theta\Delta_r)^{1/3}$. It is seen that estimated values of $\langle k_{sgs}\rangle$ develop a singularity for finer grids as one approaches to the centerline because of definition of Δ. At $x = 15D$ Fig. 5e shows two noticeable spikes in values of $\langle k_{sgs}\rangle$ around of $r = D$ which is related to the radial direction grid clustering close to the pilot and pipe walls. Overall, the adopted estimation model seems to underpredict $\langle k_{sgs}\rangle$ values and should be used with caution. In fact, as can be seen from Fig. 5e at the radial location of $r = D$ the ratio $k_{res}/\langle k_{sgs}\rangle$ is about 17 for $G1$ grid and about 29 for $G3$–$G5$ grids. This translates to approximately 94% and 97% of the resolved TKE, respectively, which seems to be too high considering given $G1$ grid resolution.

The ratio of the SGS turbulent and kinematic viscosities is shown in Fig. 6a–c for three axial locations of $x = 7.5D$, $15D$ and $45D$. This ratio can be used further to estimate the Kolmogorov length scale as $\eta = (\nu/\nu_T)^{1/2}(C_s\Delta)$ (where $C_s^2 = 0.032$ from LES of round free jets by Bogey and Bailly [44]). Radial profiles of the ratio of Δ and the mean estimated Kolmogorov scale are shown in Fig. 6d–f. The effect of the high temperature flame zone is clearly visible throughout the flow domain and manifests itself through increase in the Kolmogorov length scale due to elevated values of the kinematic viscosity. For example, at $x = 15D$ and $r = D$ the estimated ratio of $\Delta/\langle\eta\rangle$ decreases to about 2.4 on the $G5$ grid as is evident from Fig. 6e.

Finally, to evaluate the effect of the subgrid temperature fluctuations on the molecular properties we conducted two simulations on the $G1$ grid. In one simulation the molecular properties were computed with accounting for the SGS temperature variance according to Eq. (24), while in the other the SGS temperature variance was neglected which is equivalent to the assumption of $D(\widetilde{T}) = D(\widetilde{T})$. The results showed that the difference in statistics of the mixture fraction (and molecular diffusivities) fields between both cases is less than 1%. As the SGS temperature variance rapidly

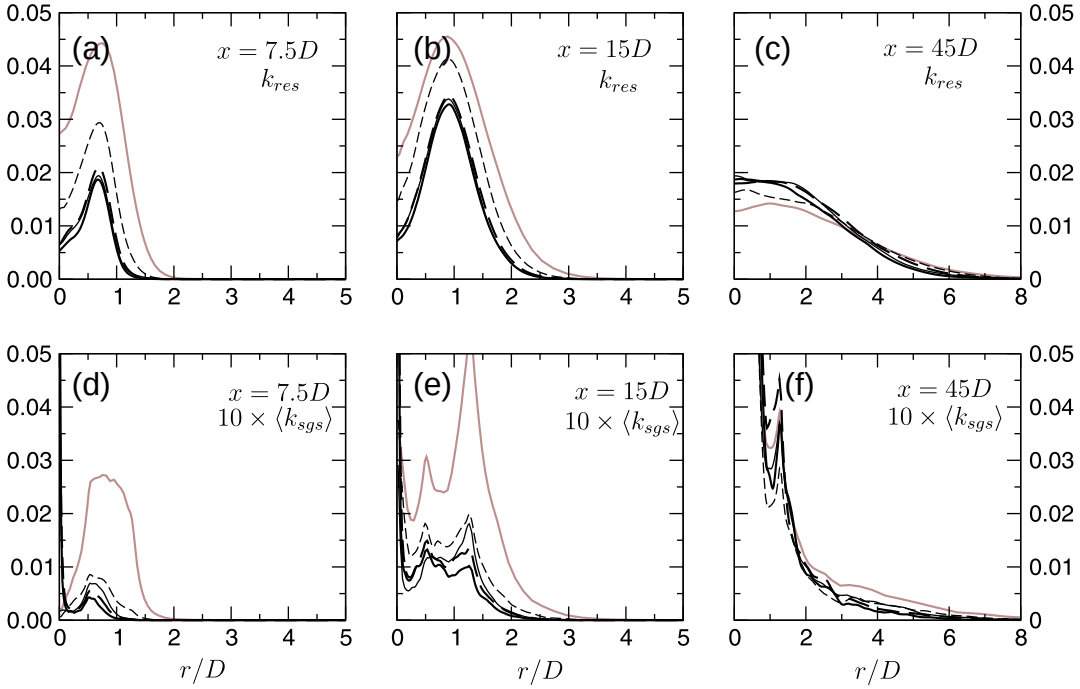

Fig. 5. Radial profiles of the resolved TKE – k_{res} (a–c) and mean SGS TKE – $\langle k_{sgs} \rangle$ (d–f) at axial locations of $x = 7.5$, $15D$ and $45D$ for different grids: $G1$ (gray), $G2$ (dashed), $G3$ (thin), $G4$ (bold dashed) and $G5$ (bold). Note that values of $\langle k_{sgs} \rangle$ are multiplied by 10 to enable comparison.

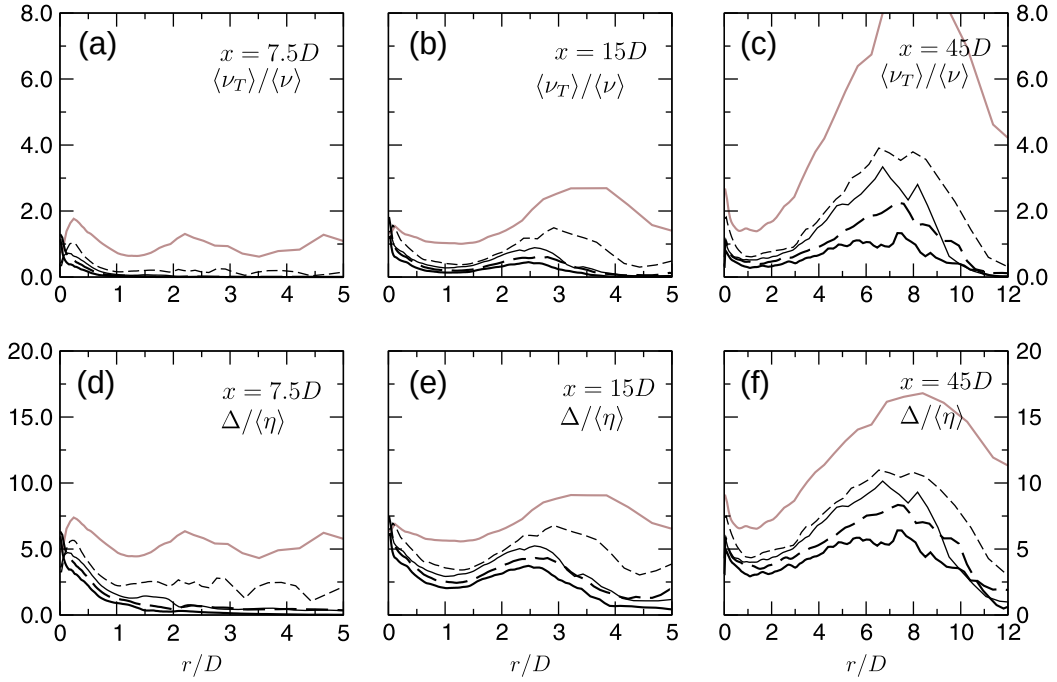

Fig. 6. Radial profiles of the ratio of $\langle \nu_T \rangle / \langle \nu \rangle$ (a–c) and the ratio of $\Delta / \langle \eta \rangle$ (d–f) ($\langle \eta \rangle$ is the estimated Kolmogorov length scale) at axial locations of $x = 7.5$, $15D$ and $45D$ for different grids: $G1$ (gray), $G2$ (dashed), $G3$ (thin), $G4$ (bold dashed) and $G5$ (bold).

decreases with the grid resolution its effect on molecular properties will be even smaller on the finer grids. As a result, in what follows we discuss results for the case of $D(\widetilde{T})$ and the effect of the SGS temperature variance is neglected.

5.2. Mixture fraction

In flamelet-based non-premixed combustion modeling the mixture fraction is an important variable since it is used to parametrize chemical composition, molecular properties and enthalpy. Therefore, it is a minimal requirement to accurately predict an evolution of the mixture fraction. Since in the present work our main focus is on molecular diffusion effects we present an abbreviated discussion of the mixture fraction field. The full analysis of the mixture fraction and velocity fields with respect to different ways of accounting for the SGS variance will be addressed in a subsequent paper.

Here, we remark that the adopted simple combustion model represents the mixture fraction field reasonably well throughout

flow domain. Figure 7a–f shows radial mean and rms mixture fraction profiles at two representative axial locations of $x = 15D$ and $30D$. In addition to the resolved rms profiles, the total mixture fraction rms (Fig. 7c and f) is computed based on additional statistical contribution from the residual motion $(\tilde{\xi}^r_{rms})^2 = \langle V_\xi \rangle$ as suggested in [13]. Both mean and rms fields exhibit good convergence to a limiting state which is reasonably well characterized by the $G3$ grid solution. The resolved rms profiles slightly underpredict the maximal values of experimental data. The contribution from the SGS variance is shown in insets of Fig. 7c and f. Qualitatively, the mean SGS variance in the radial direction shows similar behavior and convergence rate as the resolved variance but quickly becomes relatively insignificant downstream beyond $15D$.

5.3. Temperature

Since the molecular diffusivity is a function of temperature we will consider the resolved temperature field first. Axial profiles of the mean centerline temperature are shown in Fig. 8. It is seen that the mean temperature is in good agreement with the measured values for the three finest grids. The peak value is marginally underpredicted by approximately 50 K. The mean centerline temperature starts exceeding experimental values starting from a distance of $60D$ downstream. This overprediction in temperature is similar to one reported in other flamelet-based calculations and is usually attributed to not accounting for thermal radiation effects in the combustion models [24,27]. The rms temperature profiles exhibit behavior in accordance with the experimental data except beyond the location of a local minimum where the temperature fluctuations are underpredicted – a trend which was observed in some recent Flame D simulations [24,27].

Radial profiles at the intermediate locations $x = D$ through $x = 45D$ are shown in Figs. 9–12. It can be seen that mean temperature is convergent for $G3$–$G5$ grids and approximates the experimental values quite well at all axial locations. In the jet near-field (up to $x = 7.5D$) the resolved temperature is found to be convergent on the $G2$ grid also. Generally, the rms profiles of temperature give an adequate approximation to the experimental data in most of the flow domain. However, their sensitivity to the grid resolution is somewhat complicated. Downstream of $x = 15D$, the temperature rms profiles show a reasonable convergence on $G3$–$G5$ grids with a gradual deterioration at far downstream locations of $x = 45D$ and $x = 60D$, where all four grids $G2$–$G5$ are characterized by similar profiles which are insensitive to the radial resolution. As the grid is stretched downstream, the resolution in the axial direction becomes dominant and differences in the effective value of Δ among grids become less pronounced. Close to the nozzle there is noticeable convergence on $G2$, $G3$ and $G4$ grids everywhere but at the location of the rms maximum, i.e., in a mixing layer between jet fuel and hot pilot products. The finest grid $G5$, while consistent with other three up to $r = D$, shows a decrease in the temperature fluctuations in the mixing layer between pilot product and co-flow air. Figures 9–11 show that the temperature rms fluctuations tend to increase at their maxima locations in the fuel rich region as the grid resolution becomes more refined. On the other hand they exhibit an opposite behavior if their maxima are located in the lean region. A qualitatively similar pattern takes place for the rms of the mixture fraction field also (not shown). This can be explained by the interplay between the molecular and SGS diffusivities in these regions, which is briefly discussed below after presentation of molecular diffusivity results.

The square root of the mean temperature SGS variance is a measure of the unresolved temperature fluctuations which is needed to evaluate the full LES statistics. These profiles are shown in insets of Figs. 9–12. Qualitatively, they are characterized by the same pattern and less magnitudes than the resolved rms fields. It can be noted, however, that the locations of their maxima are shifted to the rich part of the jet, as it is shown in Fig. 10f, for example. As a result, the total temperature rms fluctuations have higher values close to the jet centerline.

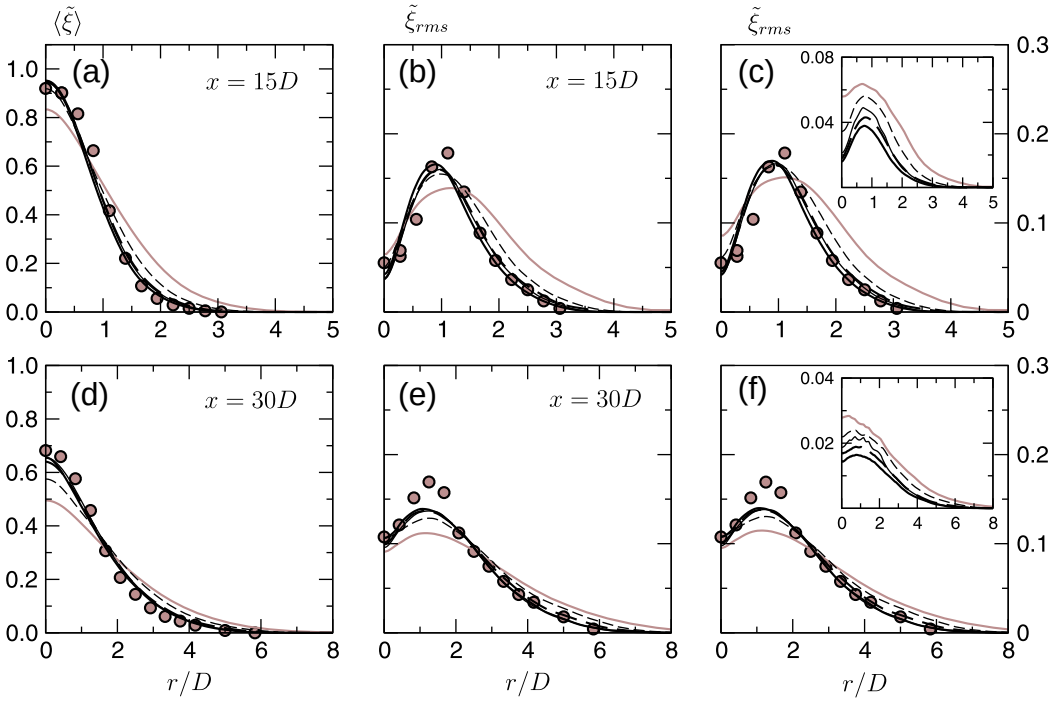

Fig. 7. Radial profiles of the mean (a and d), the resolved rms – $\tilde{\xi}^W_{rms}$ (b and e) and the total rms (c and f) $\tilde{\xi}^m_{rms} = \sqrt{\tilde{\xi}^{W2}_{rms} + \tilde{\xi}^{r2}_{rms}}$ of the mixture fraction at axial locations of $x = 15D$ and $30D$ compared with experimental data (symbols) for different grids: $G1$ (gray), $G2$ (dashed), $G3$ (thin), $G4$ (bold dashed) and $G5$ (bold). Insets in (c and f) show residual rms mixture fraction profiles, $\tilde{\xi}^r_{rms} = \sqrt{\langle V_\xi \rangle}$.

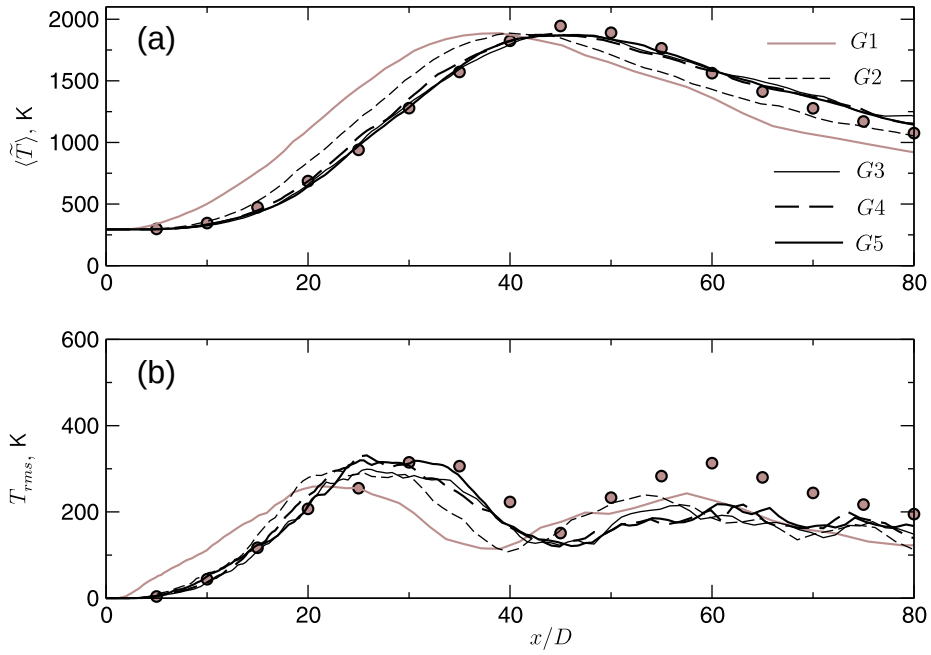

Fig. 8. Axial profiles of the centerline mean temperature (a) and the rms of temperature (b) compared with experimental data (symbols) for different grids: *G*1 (gray), *G*2 (dashed), *G*3 (thin), *G*4 (bold dashed) and *G*5 (bold).

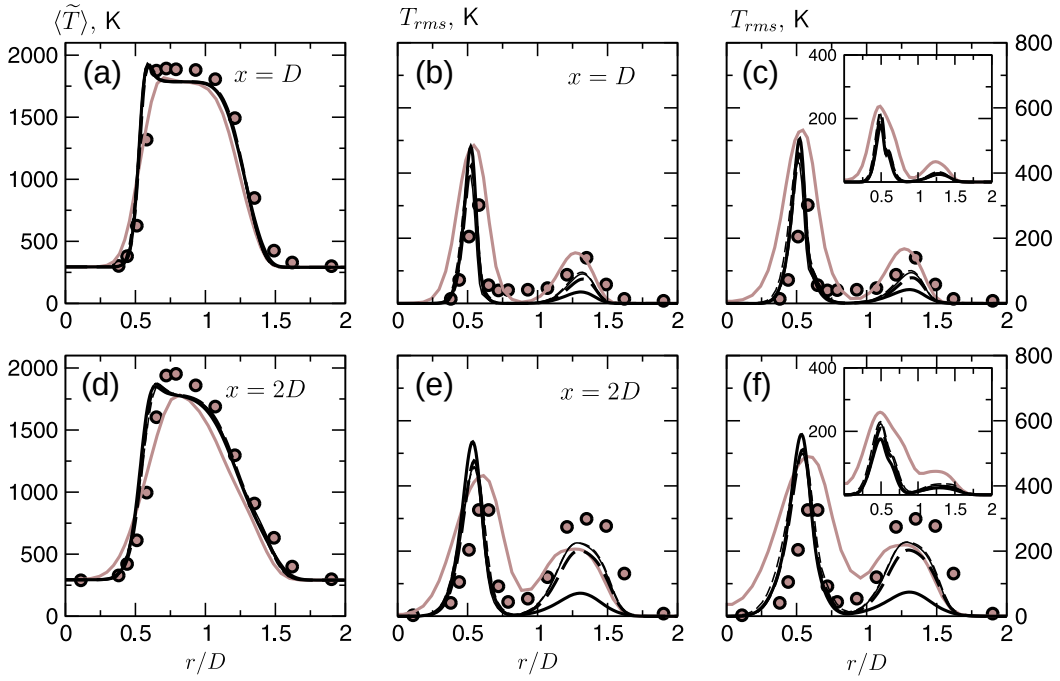

Fig. 9. Radial profiles of the mean (a and d), the resolved rms (b and e) and the total rms (c and f) of temperature at axial locations of $x = D$ and $2D$ compared with experimental data (symbols) for different grids: *G*1 (gray), *G*2 (dashed), *G*3 (thin), *G*4 (bold dashed) and *G*5 (bold). Insets (c and f) show residual rms temperature profiles, $\widetilde{T}^r_{rms} = \sqrt{\langle V_T \rangle}$.

Overall, the LES statistical results for the temperature are found to be reasonably close to the experimental data suggesting that the adopted SGS and combustion models are capable of representing the SGS effects on the temperature field for the flame considered.

5.4. Molecular diffusivity

Radial profiles of the mean molecular and turbulent subgrid diffusivities normalized by the jet reference values are shown in Figs. 13–15. The mean molecular diffusivity essentially follows temperature and is characterized by convergent behavior for *G*2–*G*5 grids. The turbulent subgrid diffusivity, on the other hand, rapidly decreases in magnitude as the grids are progressively refined. It is evident that the molecular diffusivity dominates the subgrid diffusivity in the pilot region in the near field for all grids. Even at the core of the jet (for $r \leqslant 0.5D$), the molecular diffusivity is comparable to the subgrid diffusivity up to $x = 7.5D$ for all but the coarsest grid *G*1. Thus, the molecular diffusivity is an important

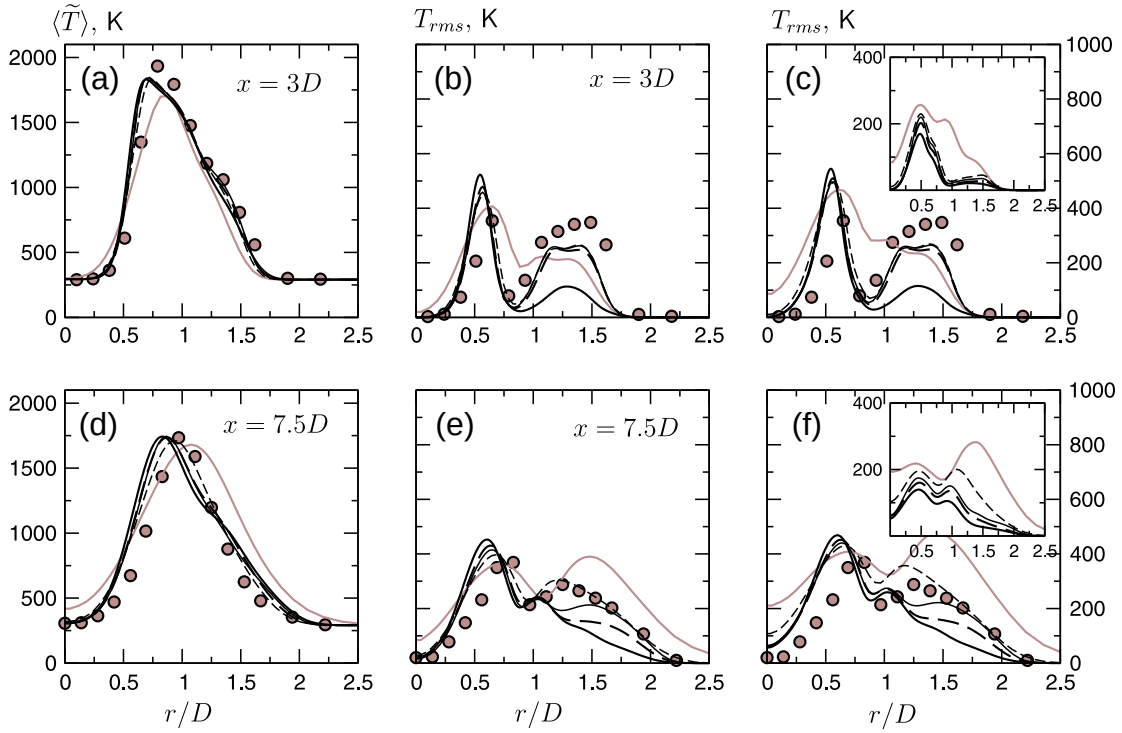

Fig. 10. Radial profiles of the mean (a and d), the resolved rms (b and e) and the total rms (c and f) of temperature at axial locations of $x = 3D$ and $7.5D$ compared with experimental data (symbols) for different grids: $G1$ (gray), $G2$ (dashed), $G3$ (thin), $G4$ (bold dashed) and $G5$ (bold). Insets (c and f) show residual rms temperature profiles, $\widetilde{T}^r_{rms} = \sqrt{\langle V_T \rangle}$.

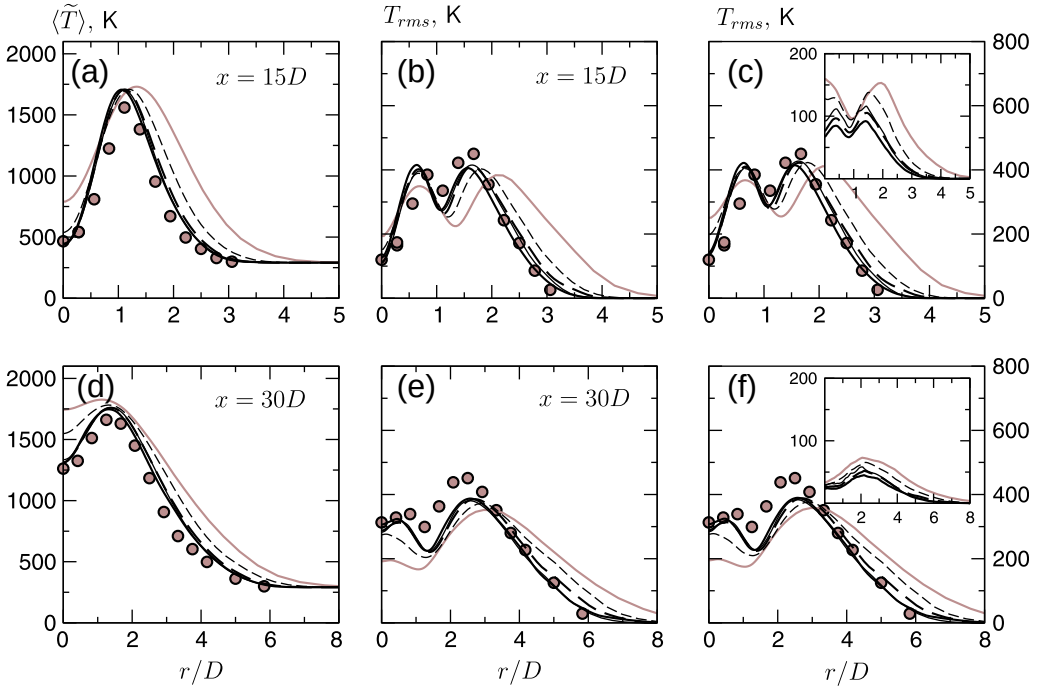

Fig. 11. Radial profiles of the mean (a and d), the resolved rms (b and e) and the total rms (c and f) of temperature at axial locations of $x = 15D$ and $30D$ compared with experimental data (symbols) for different grids: $G1$ (gray), $G2$ (dashed), $G3$ (thin), $G4$ (bold dashed) and $G5$ (bold). Insets (c and f) show residual rms temperature profiles, $\widetilde{T}^r_{rms} = \sqrt{\langle V_T \rangle}$.

factor for the initial (close to the nozzle) flow pattern development. It is remarked that jet flames can be affected significantly by changes in the exit flow pattern as they propagate downstream retaining the near-field "memory" [45]. As the jet develops the turbulent subgrid diffusivity starts overcoming the molecular diffusivity downstream after about a distance of $30D$ at the radial locations greater than approximately $3D$ which is depicted in Fig. 15. Nevertheless, the molecular diffusivity remains significant throughout the flow domain up to radial distance of $4D$ for all reasonably resolved grids.

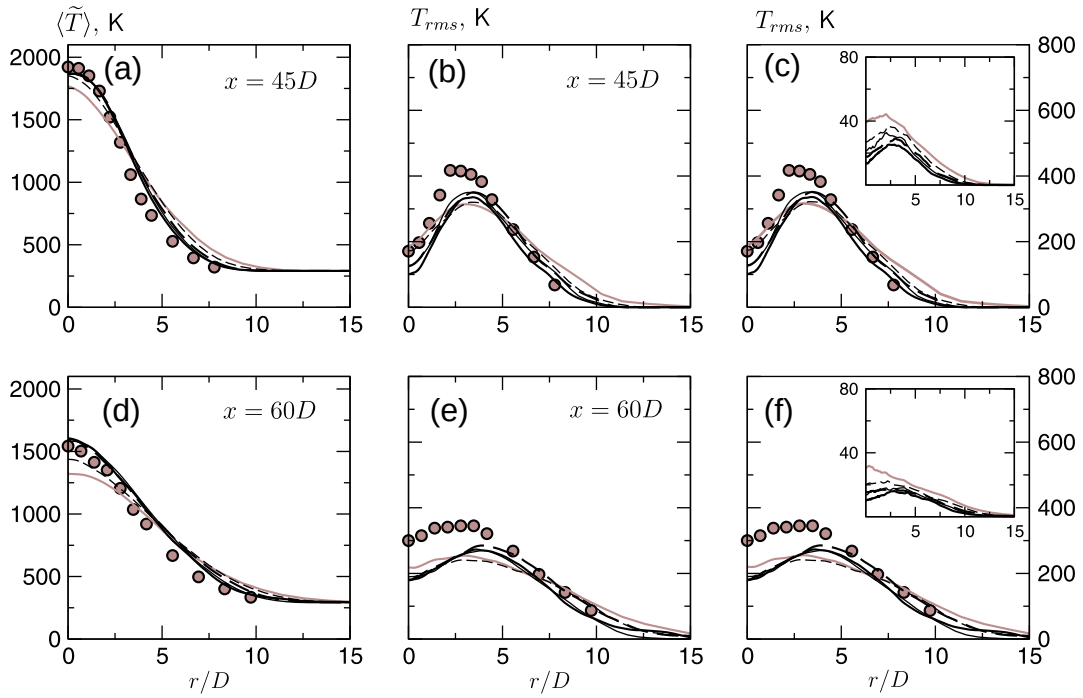

Fig. 12. Radial profiles of the mean (a and d), the resolved rms (b and e) and the total rms (c and f) of temperature at axial locations of $x = 45D$ and $60D$ compared with experimental data (symbols) for different grids: $G1$ (gray), $G2$ (dashed), $G3$ (thin), $G4$ (bold dashed) and $G5$ (bold). Insets (c and f) show residual rms temperature profiles, $\widetilde{T}^{r}_{rms} = \sqrt{\langle V_T \rangle}$.

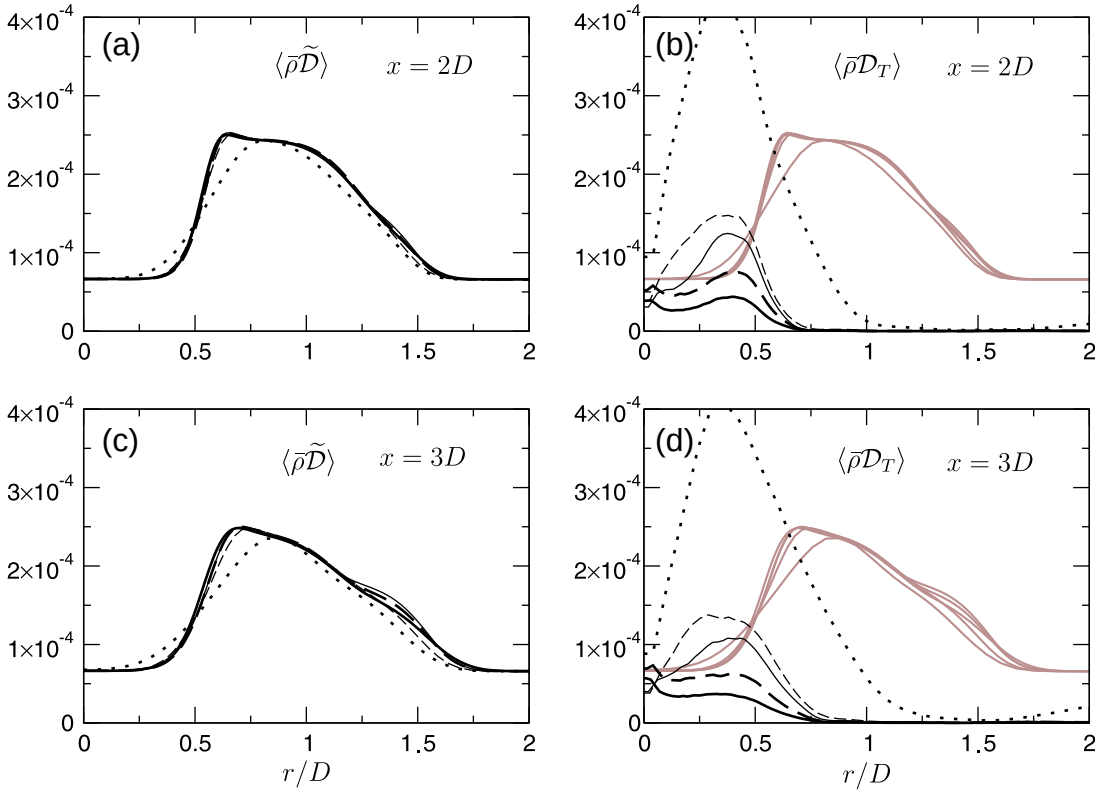

Fig. 13. Radial profiles of the molecular (a and c) and turbulent subgrid (b and d) diffusivities at axial locations $x = 2D$ and $x = 3D$ for different grids: $G1$ (dots), $G2$ (dashed), $G3$ (thin), $G4$ (bold dashed) and $G5$ (bold). Note that profiles of molecular diffusivity are also shown in (b and d) as gray lines to enable comparison.

We note that the turbulent subgrid diffusivity shows somewhat artificially high levels very near the centerline as the jet develops downstream. The finer grid is employed the earlier the turbulent subgrid diffusivity starts exhibiting this behavior. Such a peculiarity can be attributed to the excessive values of the Smagorinsky constant close to the centerline in regions where the resolved

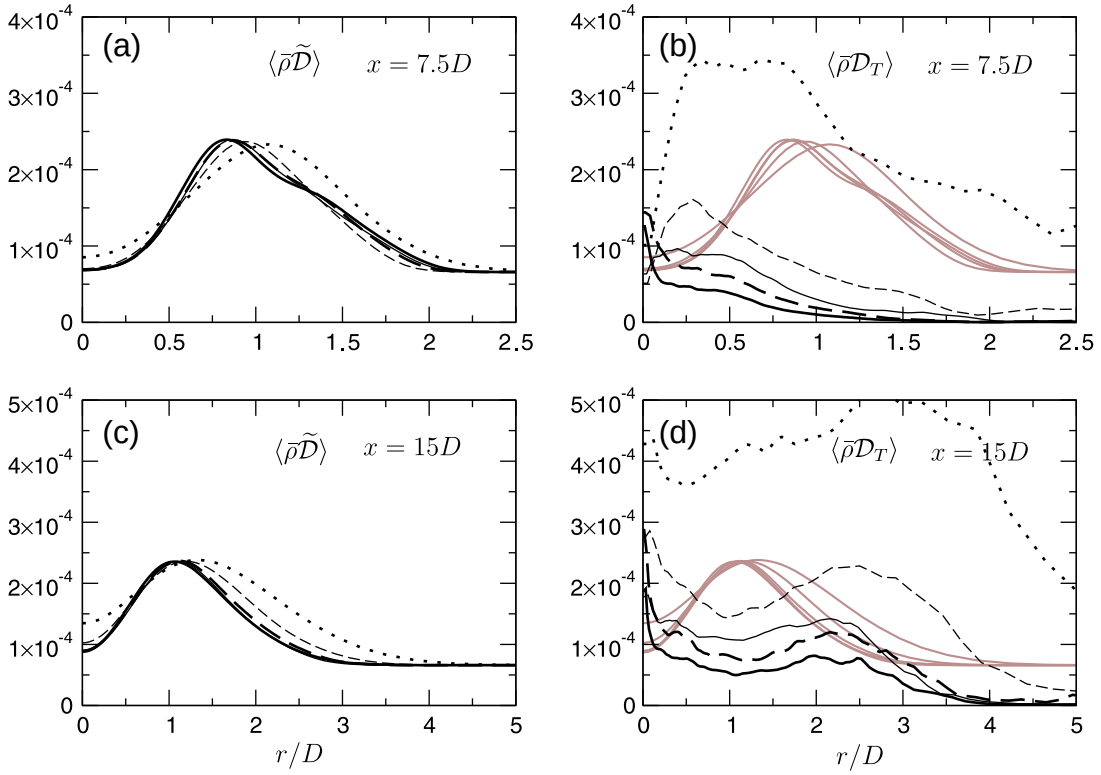

Fig. 14. Radial profiles of the molecular (a and c) and turbulent subgrid (b and d) diffusivities at axial locations $x = 7.5D$ and $x = 15D$ for different grids: $G1$ (dots), $G2$ (dashed), $G3$ (thin), $G4$ (bold dashed) and $G5$ (bold).

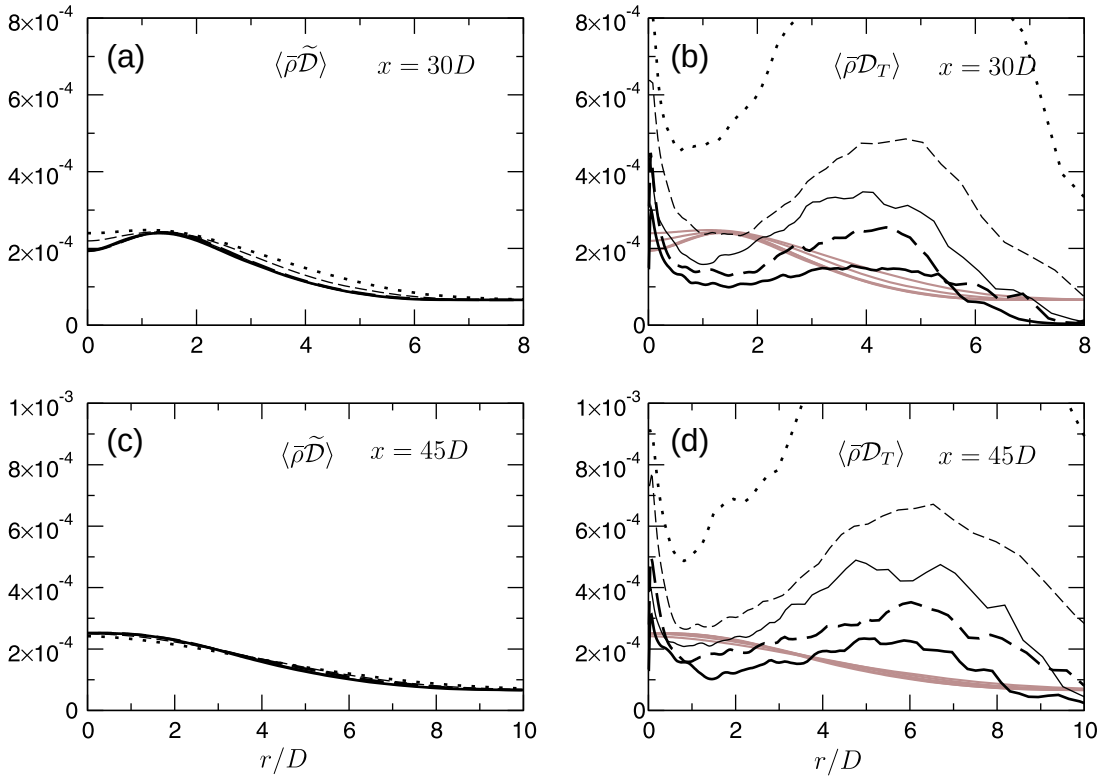

Fig. 15. Radial profiles of the molecular (a and c) and turbulent subgrid (b and d) diffusivities at axial locations $x = 30D$ and $x = 45D$ for different grids: $G1$ (dots), $G2$ (dashed), $G3$ (thin), $G4$ (bold dashed) and $G5$ (bold).

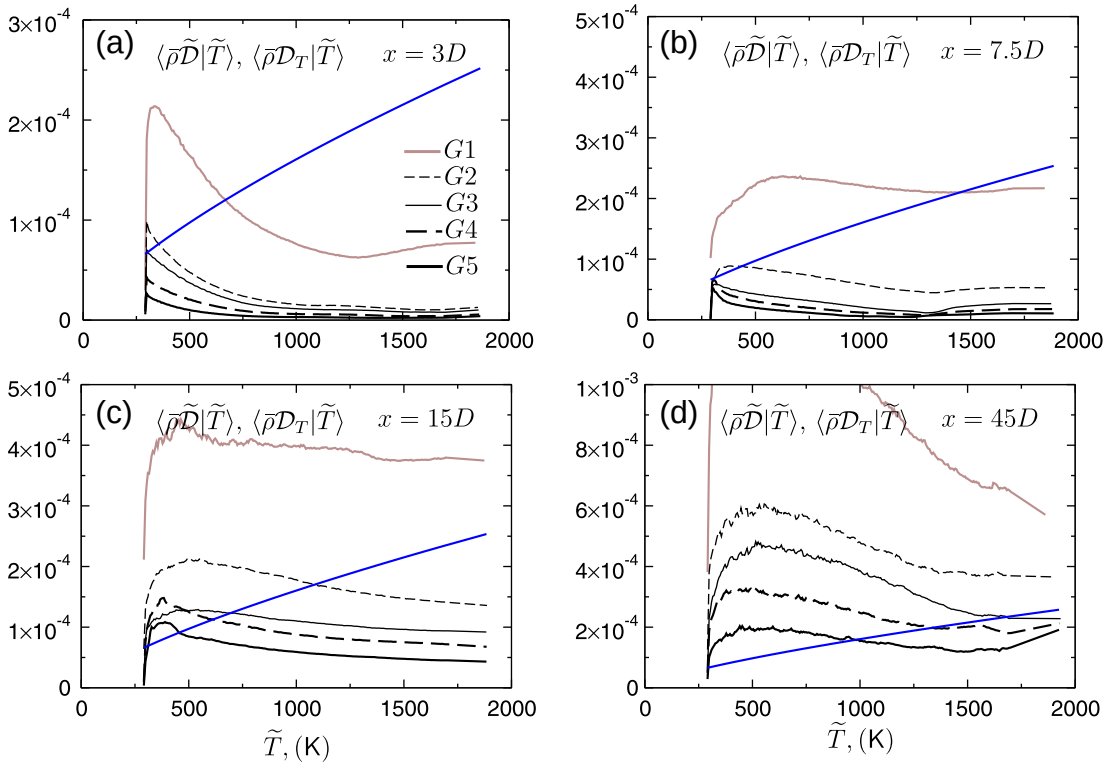

Fig. 16. Conditional means of molecular (monotonic line) and turbulent subgrid diffusivities at axial locations of $x = 3D$, $7.5D$, $15D$ and $45D$ for different grids. Note that profiles of conditional molecular diffusivities are essentially coincident.

velocity gradients are not high and show small changes in magnitude when they are computed at the test filter level. As a result, the denominator in the Smagorinsky constant definition that depends on the difference between the test-filtered strain rate $|\widehat{\widetilde{S}}|\widehat{\widetilde{S}}_{ij}$ (multiplied by the square of the ratio of the test to grid level filters) and the test-filtered resolved strain rate $\widehat{|\widetilde{S}|\widetilde{S}}_{ij}$ becomes small. The primary cause for this in the current simulations is the specification of the turbulence resolution scale which is taken to be $\Delta = (\Delta_x\Delta_\theta)^{1/2}$, thus independent of resolution in the radial direction. Correspondingly, the test filtering is performed only in the axial and circumferential directions. It is expected that accounting for Δ_r and filtering in the radial direction will alleviate this behavior of the subgrid viscosity, and therefore, diffusivity near the axis by increasing the difference between corresponding strain rate tensors.

Figure 13 provides a qualitative explanation why the maximum values of the mixture fraction and temperature rms fields increase with the grid resolution in the jet rich region ($r \sim 0.5D - 0.6D$). Here, the mixture fraction gradient in the radial direction is quite large and is adequately resolved on all $G2$–$G5$ grids, as follows from the convergence of the mixture fraction at this locations. The turbulent subgrid diffusivity is comparable with the molecular diffusivity and decreases strongly as one goes from $G2$ to $G5$. As a result, the total diffusivity $\bar{\rho}(\widetilde{\mathscr{D}} + \mathscr{D}_T)$ is also decreasing which produces less dissipation for finer grids and promotes higher values of the rms of the mixture fraction and temperature. On the other hand, in the lean region ($r \sim 1.0D - 1.5D$), the molecular diffusivity is much higher than the subgrid one, ($\bar{\rho}\widetilde{\mathscr{D}} \gg \bar{\rho}\mathscr{D}_T$), and essentially is the same for all $G2$–$G5$ grids due to convergence. The mixture fraction gradient in the radial direction is much less than in a mixing layer between the jet fuel and the pilot products and more sensitive to grid resolution. Higher values of the mixture fraction gradient on finer grids tend to increase the scalar dissipation which damps the rms fluctuations, while the role of the diffusion coefficient remains rather passive.

The relative importance of the molecular diffusivity can be further highlighted by considering conditional statistics. Figure 16a–d shows conditional means of the molecular and SGS diffusivities with respect to temperature at four axial locations from $x = 3D$ to $x = 45D$. Conditional means are computed at each axial location by binning temperature with a bin size of 6 K and taking the sample average of the accumulated diffusivity data in each bin.

It is seen that in the jet near-field, up to $x = 7.5D$, the molecular diffusivity dominates the turbulent SGS diffusivity except at low temperatures (less 500 K) and on the very coarse grid $G1$. For grids $G3$–$G5$ the molecular diffusivity always exceeds its turbulent counterpart for the whole temperature range. Farther downstream, at $45D$, on the finest grid $G5$, the molecular diffusivity dominates the turbulent diffusivity for temperatures above 1000 K.

6. Conclusions

LES of the piloted non-premixed Sandia flame D have been performed on a series of grids with progressively increasing resolution from 0.19 to 10.4 million cells, with the purpose of studying the molecular diffusion effects in LES of a piloted methane–air flame. The importance of the molecular diffusivity in the correct representation of spatial transport has a profound effect on LES/PDF combustion modeling.

In the present effort, a simple combustion model has been proposed to parametrize reacting density and temperature in terms of the mixture fraction and subgrid scale variance using quadratic B-splines. As a result, two transport equations for these scalars need to be integrated. Quadratic B-splines analytic approximations of specific volume and temperature have been obtained based on a

flamelet CHEMKIN simulation with a detailed chemistry mechanism. These approximations eliminate the effect of interpolation uncertainties on an LES solution. To study the LES statistics of temperature, a model for the SGS temperature variance has been formulated and tested. The model requires specification of the third and the fourth SGS moments which were modeled by a standard beta-pdf distribution. Generally, the adopted combustion model is found to be capable to reproduce essential features of the temperature field in Sandia flame D, especially on fine grids. The mean temperature field exhibits grid convergence throughout the whole flow domain, while the rms of the temperature is found to be non-convergent in regions where it attains its local maximum values.

After having established an adequate prediction of the temperature field, we analyzed the molecular diffusivity and compared it to the turbulent subgrid diffusivity. Statistical results show that the molecular diffusivity is important in the near-field of the jet where it exceeds or is comparable to the turbulent subgrid diffusivity on all reasonably resolved grids. As the region with the high turbulent diffusivity grows farther downstream and moves away from the centerline, the molecular diffusivity remains comparable in magnitude up to a distance of $4D$ in the radial direction. Finally, the conditioning on temperature demonstrates the similar finding as the flow-field analysis. The conditional mean values of the molecular diffusivity always exceed the corresponding mean values of the turbulent subgrid diffusivity in the near field except for the two coarsest grids $G1$ and $G2$ and at low temperatures, less than 500 K. Overall, the results obtained suggest that molecular transport should be treated accurately in LES combustion models in order to correctly predict essential features of jet flames.

Acknowledgments

This work was supported by the Air Force Office of Scientific Research under Grant No. FA-9550-09-1-0047. This research was also supported in part by the National Science Foundation through TeraGrid resources provided by Texas Advanced Computing Center under Grant No. TG-CTS090020.

References

[1] S.B. Pope, Proc. Combust. Inst. 23 (1990) 591–612.
[2] S. Menon, P.A. McMurtry, A.K. Kerstein, in: Large-eddy simulation of Complex and Geophysical Flows, Cambridge University Press, 1993.
[3] S. Navarro-Martinez, A. Kronenburg, F. di Mare, Flow, Turbul. Combust. 75 (2005) 245–274.
[4] A.Y. Klimenko, Phys. Fluids 21 (2009) 065102.
[5] K. Mahesh, G. Constantinescu, S. Apte, G. Iaccarion, F. Ham, P. Moin, J. Appl. Mech. 73 (2006) 374–381.
[6] G. Boudier, L.Y.M. Gicquel, T.J. Poinsot, Combust. Flame 155 (2008) 196–214.
[7] S.B. Pope, Prog. Energy Combust. Sci. 11 (1985) 119–192.
[8] R.R. Cao, S.B. Pope, Combust. Flame 143 (2005) 450–470.
[9] Z. Ren, S.B. Pope, Proc. Combust. Inst. 32 (2009) 1629–1637.
[10] P.J. Colucci, F.A. Jaberi, P. Givi, S.B. Pope, Phys. Fluids 10 (1998) 499–515.
[11] S.B. Pope, J. Fluid Mech. 652 (2010) 139–169.
[12] R. McDermott, S.B. Pope, J. Comput. Phys. 226 (2007) 947–993.
[13] S.B. Pope, New J. Phys. 6 (2004) 35.
[14] R.S. Barlow, J.H. Frank, Proc. Combust. Inst. 27 (1998) 1087–1095.
[15] C. Schneider, A. Dreizler, J. Janicka, E.P. Hassel, Combust. Flame 135 (2003) 185–190.
[16] H. Pitsch, H. Steiner, Phys. Fluids 12 (2000) 2541–2554.
[17] H. Pitsch, Proc. Combust. Inst. 29 (2002) 1971–1978.
[18] A. Kempf, F. Flemming, J. Janicka, Proc. Combust. Inst. 30 (2005) 557–565.
[19] M.R.H. Sheikhi, T.G. Drozda, P. Givi, F.A. Jaberi, S.B. Pope, Proc. Combust. Inst. 30 (2005) 549–556.
[20] R. Mustata, L. Valino, C. Jimenez, W.P. Jones, S. Bondi, Combust. Flame 145 (2006) 88–104.
[21] V. Raman, H. Pitsch, Proc. Combust. Inst. 31 (2007) 1711–1719.
[22] S. James, J. Zhu, M.S. Anand, Proc. Combust. Inst. 31 (2007) 1737–1745.
[23] J.-Y. Chen, Combust. Theory Modell. 11 (2007) 675–695.
[24] M. Ihme, H. Pitsch, Combust. Flame 155 (2008) 90–107.
[25] D.J. Clayton, W.P. Jones, Flow, Turbul. Combust. 81 (2008) 497–521.
[26] S.A. Ferraris, J.X. Wen, Flow, Turbul. Combust. 75 (2008) 245–274.
[27] A.W. Vreman, B.A. Albrecht, J.A. van Oijen, L.P.H. de Goey, R.J.M. Bastiaans, Combust. Flame 153 (2008) 394–416.
[28] N. Peters, Prog. Energy Combust. Sci. 10 (1984) 319–339.
[29] C.D. Pierce, P. Moin, J. Fluid Mech. 504 (2004) 73–97.
[30] R.W. Bilger, AIAA J. 20 (1982) 962–970.
[31] E. Giacomazzi, F.R. Picchia, N. Arcidiacono, Combust. Theory Modell. 12 (2008) 135–158.
[32] H. Pitsch, N. Peters, Combust. Flame 114 (1998) 26–40.
[33] L. Shunn, P. Moin, Large-eddy simulation of combustion systems with convective heat-loss, Technical Report, Stanford University, 2009, Report No. TF-111.
[34] C. Pera, J. Réveillon, L. Vervisch, P. Domingo, Combust. Flame 146 (2006) 635–648.
[35] A.W. Cook, J.J. Riley, Combust. Flame 112 (1998) 593–606.
[36] M. Germano, U. Piomelli, P. Moin, W.H. Cabot, Phys. Fluids A 3 (1991) 1760–1765.
[37] D.K. Lilly, Phys. Fluids A 4 (1992) 633–635.
[38] P. Domingo, L. Vervisch, D. Veynante, Combust. Flame 152 (2008) 415–432.
[39] C.R. Wilke, J. Chem. Phys. 18 (1950) 517–519.
[40] A.W. Cook, J.J. Riley, Phys. Fluids 6 (1994) 2868–2870.
[41] R.W. Bilger, S.H. Stårner, R. Kee, Combust. Flame 90 (1990) 135–149.
[42] B.P. Leonard, Comput. Methods Appl. Mech. Eng. 19 (1979) 59–98.
[43] I. Celik, M. Klein, J. Janicka, J. Fluids Eng. 131 (2009) 031102.
[44] C. Bogey, C. Bailly, Int. J. Heat Fluid Flow 27 (2006) 603–610.
[45] G.J. Nathan, J. Mi, Z.T. Alwahabi, G.J.R. Newbold, D. Nobes, Prog. Energy Combust. Sci. 32 (2006) 496–538.